RSC Advances

PAPER

View Article Online
View Journal | View Issue

Check for updates

Cite this: *RSC Adv.*, 2017, 7, 37975

Received 11th July 2017
Accepted 25th July 2017

DOI: 10.1039/c7ra07636c

rsc.li/rsc-advances

Steric effect on Li$^+$ coordination and transport properties in polyoxetane-based polymer electrolytes bearing nitrile groups†

Ryansu Sai,[a] Kazuhide Ueno, *[b] Kenta Fujii, [a] Yohei Nakano‡[a] and Hiromori Tsutsumi*[a]

Polymer electrolytes (PEs) that consist of polyoxetane with nitrile side chains and lithium bis(trifluoromethanesulfonyl)amide were studied as electrolytes for Li secondary batteries. Our previous study showed that Li$^+$ ion coordination with the polar nitrile groups tethered to the main chain plays a crucial role in enhancing the Li$^+$ ion transport properties in poly(3-(2-cyanoethoxymethyl)-3-ethyloxetane) (PCEO). Herein, we report the effects of the absence of ethyl groups on the main chain of PCEO on Li$^+$ ion coordination, thermal properties, and ionic transport, by employing a structural analog, poly(3-(2-cyanoethoxymethyl)-oxetane). We found that the steric hindrance derived from the ethyl groups in PCEO resulted in more-pronounced Li$^+$ coordination with the nitrile side chains, and thereby more effective Li$^+$ ion transport was achieved. We also demonstrated successful charge/discharge cycling of a Li/LiFePO$_4$ cell using nitrile-functionalized PE.

1. Introduction

There has been much effort to develop solid-state electrolytes, including inorganic and polymeric electrolytes, with high ionic conductivities as alternatives to liquid electrolytes in electrochemical devices.[1,2] Recent breakthroughs in inorganic solid electrolytes have remarkably improved the conductivity, which is now comparable to or even higher than that of liquid electrolytes.[3] This has led to a burgeoning field of study for all-solid-state lithium-ion batteries with high energy and power densities, long cycle lives, and safety for use in automotive and other large-scale energy storage.[4] Meanwhile, the ionic conductivities of polymer electrolytes (PEs) are less than those of liquid electrolytes by orders of magnitude, and they are still insufficient for practical battery applications despite numerous studies.[5] Alternatively, PEs have several advantageous properties over inorganic solid electrolytes.[6] Their inherent flexibility and processability enable formation of more effective electrode/electrolyte interfaces in the composite electrodes of batteries, which is a challenge in all-solid-state batteries that use solid ceramic electrolytes.[7] Flexible PEs would be more tolerant to electrode volume changes during charge/discharge (especially for conversion reactions). Moreover, PEs generally possess higher stabilities than many of the solid ceramic electrolytes at low potentials for negative electrodes, such as lithium metal.

The most well-studied lithium-conductive PEs have been based on a binary mixture of poly(ethylene oxide) (PEO) and lithium salts since ionic conduction was first reported for alkali metal salts dissolved in PEO,[8] whereby polyether chains form a complex with metal cations.[9] The migration of metal cations is strongly coupled with the segmental motion of the polyether chains; thus, PEO-based PEs generally show low ionic conductivities. To improve the ionic conduction in PEs, many types of modified polymer matrices, such as random copolymer, block copolymer, comb-type copolymer, and polymer blends, have been studied.[6] Polyoxetanes are polyethers that contain trimethylene oxide units and can also be used as a polymer matrix for PEs.[10–12] PEs based on polyoxetanes with polar side chains, such as nitrile groups and phosphate ester groups, were reported.[13–15] The increase in glass transition temperature (T_g) associated with complexation with Li$^+$ ions, which is a typical behavior for PEs, does not occur in poly(3-(2-cyanoethoxymethyl)-3-ethyloxetane) (PCEO); rather, T_g decreases with increasing salt concentration.[16] This could be caused by steric hindrance of the ethyl groups on the main chain and preferential Li$^+$ ion coordination with the nitrile side chains. We confirmed that Li$^+$ ion coordination with the nitrile groups in PCEO is responsible for improving the ionic transport properties of the PEs.[17]

---

[a] *Department of Applied Chemistry, Graduate School of Sciences and Technology for Innovation, Yamaguchi University, 2-16-1 Tokiwadai, Ube, 755-8611, Japan. E-mail: tsutsumi@yamaguchi-u.ac.jp; Fax: +81-836-85-9282/9201; Tel: +81-836-85-9282/9201*

[b] *Department of Chemistry and Biotechnology, Yokohama National University, 79-5 Tokiwadai, Hodogaya-ku, Yokohama, 240-8501, Japan. E-mail: ueno-kazuhide-rc@ynu.ac.jp; Fax: +81-45-339-3951; Tel: +81-45-339-3951*

† Electronic supplementary information (ESI) available. See DOI: 10.1039/c7ra07636c

‡ Present address: Department of Materials and Life Sciences, Sophia University, 7-1 Kioi-cho, Chiyoda-ku, Tokyo, 102-8554, Japan.

In this study, poly(3-(2-cyanoethoxymethyl)-oxetane) (PCHO) was newly synthesized. The only difference between PCEO and PCHO is the absence of an ethyl group on the polyoxetane main chain. To clarify the contribution of the ethyl group to the electrolyte properties such as the ionic conductivity (σ) and lithium transference number (t_{Li^+}), PCHO complexed with lithium bis(trifluoromethanesulfonyl)amide (LiTFSA) were evaluated and were compared with previously reported PCEO electrolytes.[17] Here, we verified that subtle changes in the chemical structure of the repeating monomer unit of the polyoxetane-based PEs (*i.e.*, the presence or absence of the ethyl group on the main chain) greatly affected the thermal properties and ionic transport, which were well correlated with different Li^+ ion coordination structures studied by Raman spectroscopy. A Li/$\mathrm{LiFePO_4}$ cell was fabricated and its charge/discharge behavior was examined to demonstrate the applicability of the polyoxetane-based PEs to lithium secondary batteries.

2. Experimental section

2.1 Preparation of the monomer

An oxetane derivative, 3-(2-cyanoethoxymethyl)-oxetane (CHO), was synthesized by Michael addition. 3-Oxetanemethanol (5.64 mL, 70.0 mmol) and acrylonitrile (5.24 mL, 80.0 mmol) were mixed with a 20% tetraethylammonium hydroxide solution (0.6 mL) as a catalyst in pure water (3 mL), then stirred at room temperature overnight. The reaction mixture was extracted with chloroform, and the organic phase was washed with a large amount of water. After removal of chloroform by a rotary evaporator, the obtained liquid was applied to a silica column (eluent = ethyl acetate : hexane, 7 : 3). The product was obtained by removing the eluent and vacuum drying at 60 °C (yield: 3.54 g, 35.9%). The synthesized CHO was characterized using time-of-flight mass spectrometry, and ^{1}H and ^{13}C nuclear magnetic resonance (NMR) spectroscopy. The density of the monomer was 1.068 g cm^{-3}.

CHO ^{1}H NMR (δ, ppm from tetramethylsilane (TMS) in $\mathrm{CDCl_3}$): 2.62 (t, 2H, J = 6.00 Hz, $-\mathrm{CH_2}-\mathrm{CN}$), 3.24 (sep., 1H, J = 5.8 Hz, $-(\mathrm{CH_2})_3-\mathrm{CH}$), 3.70 (t, 2H, J = 6.0 Hz, $-\mathrm{CH_2}-\mathrm{CH_2}-\mathrm{CN}$), 3.75 (d, 2H, J = 7.0 Hz, $-\mathrm{CH}-\mathrm{CH_2}-\mathrm{O}-$), 4.46 (t, 2H, J = 6.3 Hz, ring, $-\mathrm{CH_2}-\mathrm{O}-\mathrm{CH_2}-$), 4.81 (dd, 2H, J = 1.0 Hz, 6.0 Hz, ring, $-\mathrm{CH_2}-\mathrm{O}-\mathrm{CH_2}-$).

CHO ^{13}C NMR (δ, ppm from TMS in $\mathrm{CDCl_3}$): 18.52 ($-\mathrm{CH_2}-\mathrm{CN}$), 34.45 ($(\mathrm{CH_2})_2-\mathrm{CH_2}-\mathrm{CH_3}$), 65.39 ($-\mathrm{CH_2}-\mathrm{CH_2}-\mathrm{CN}$), 72.34 ($-\mathrm{CH}-\mathrm{CH_2}-\mathrm{O}-$), 74.03 ($-\mathrm{CH_2}-\mathrm{O}-\mathrm{CH_2}-$), 117.61 ($-\mathrm{CN}$).

2.2 Preparation of the polymer

CHO was polymerized by a ring-opening cationic polymerization using $\mathrm{BF_3 \cdot Et_2O}$ as a cationic initiator. CHO (2.42 mL, 18.3 mmol) and the initiator (50.2 μL, 0.400 mmol) were dissolved in dichloroethane (total volume: 5 mL). The polymerization was performed under an Ar atmosphere at 0 °C for 6 h in a salt ice bath. The reaction was quenched with the addition of aqueous 4 M NaCl/1 M NaOH (5 mL). The reaction mixture was added to chloroform, and the solution was washed with water. After removing chloroform using a rotary evaporator, the mixture was poured into a large amount of 2-propanol to precipitate the polymerized CHO (PCHO). The resulting polymer was collected by filtration and dried at 100 °C under vacuum (yield: 2.17 g, 84.1%). The chemical structures of PCEO (reported in our previous study) and PCHO are shown in Fig. 1.

PCHO ^{1}H NMR (δ, ppm from TMS in $\mathrm{CDCl_3}$): 2.15 (quin., 1H, J = 5.9 Hz, $(\mathrm{CH_2})_3-\mathrm{CH}$), 2.61 (t, 2H, J = 6.3 Hz, $-\mathrm{CH_2}-\mathrm{CN}$), 3.43 (m, 4H, $-\mathrm{O}-\mathrm{CH_2}-\mathrm{CH}-$), 3.53 (d, 2H, J = 6.0 Hz, $-\mathrm{CH}-\mathrm{CH_2}-\mathrm{O}-$), 3.64 (t, 2H, J = 6.0 Hz, $-\mathrm{CH_2}-\mathrm{CH_2}-\mathrm{CN}$).

PCHO ^{13}C NMR (δ, ppm from TMS in $\mathrm{CDCl_3}$): 18.85 ($-\mathrm{CH_2}-\mathrm{CN}$), 40.20 ($(\mathrm{CH_2})_3-\mathrm{CH}$), 65.63 ($-\mathrm{CH_2}-\mathrm{CH_2}-\mathrm{CN}$), 69.29 ($-\mathrm{CH}-\mathrm{CH_2}-\mathrm{O}-$), 69.38 ($-\mathrm{CH_2}-\mathrm{O}-\mathrm{CH}-$), 118.13 ($-\mathrm{CN}$).

2.3 Preparation of polymer electrolytes

The PEs were prepared using a solvent casting method. PCHO and 1 M LiTFSA in a tetrahydrofuran (THF) solution were mixed and then heated under vacuum to completely remove THF. In this report, the molar ratio of the repeating monomer unit to LiTFSA is represented as "a" (a = 40, 30, 20, 10, 5, and 3) for PCHO_aLiTFSA. The concentrations of LiTFSA (c_{Li}) in PCHO_a-LiTFSA were estimated using the corresponding monomer density (1.068 g cm^{-3}) and the reported density of molten LiTFSA (1.970 g cm^{-3}).[18] The high temperature data for the density of molten LiTFSA were extrapolated to room temperature. We assumed the additivity of the volumes of the monomers and LiTFSA when calculating the density of the PEs.

2.4 Measurements

^{1}H and ^{13}C NMR spectra of the synthesized substances were recorded using a Fourier transform NMR spectrophotometer (JNM-LA500, JEOL). The molecular weight of the polymer was measured using a gel permeation chromatography (GPC) system (SCL-10AVP, LC-10ADVP, DGU-12A, CTO-10AVP, and RID-10A, Shimadzu). GPC was performed using THF as the elution solvent and polystyrene standards to calibrate the columns.

A differential scanning calorimeter (DSC7020, HITACHI) was used to determine the glass transition temperature (T_g). A small amount of the PEs (∼10 mg) was hermetically sealed in an aluminum differential scanning calorimetry (DSC) pan. The samples were heated to 120 °C, cooled to −120 °C, and heated again to 120 °C at a heating/cooling rate of 10 °C min^{-1}. The second heating scan was recorded as the DSC thermogram of the samples. T_g was determined as the onset of the heat flow step.

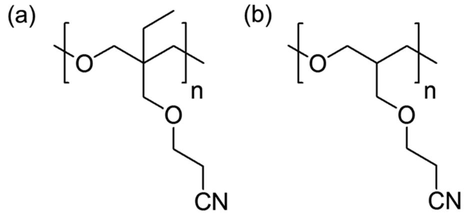

Fig. 1 Structures of the matrix polymers: (a) PCEO and (b) PCHO.

The ionic conductivity of the PEs was measured by ac impedance spectroscopy using a potentio/galvanostat (SP-150, BioLogic). The PE was placed between two stainless steel electrodes and separated by a polytetrafluoroethylene ring spacer; the conductivity cell (swagelok cell) was thermally equilibrated in a temperature cabinet (LU-14, ESPEC) at each temperature (temperature range: 20–90 °C) for 1 h before the measurements. The conductivity values were calculated using the thickness and inner diameter of the ring spacer filled with the PEs.

Raman spectra of the PEs were measured using a laser Raman spectrophotometer (NRS-3100, JASCO) with a 532 nm laser. The PE was sealed between two glass plates with a rubber spacer (thickness: 5 mm) in an Ar-filled glove box to avoid moisture adsorption. Raman spectra of PCHO$_a$LiTFSA were measured from 500–2400 cm^{-1} with a resolution of 4 cm^{-1}. The obtained spectra were normalized with respect to the methylene vibration of polyoxetanes (1390–1520 cm^{-1}) and were analyzed using commercial software for peak fitting (PeakFit™ version 4.12, SYSTAT). A pseudo-Voigt function was used for peak deconvolution.

The transference numbers of Li ions (t_{Li^+}) in PCHO$_5$LiTFSA and PCEO$_5$LiTFSA (the sample reported in the previous report,[17] $M_\mathrm{n} = 4.56 \times 10^4$ g mol^{-1}) were determined using the electrochemical method proposed by Bruce and Vincent.[19] The required parameters were obtained using potentiostatic polarization and ac impedance spectroscopy with a potentio/galvanostat (SP-150, BioLogic). The PE was placed between two lithium foil electrodes that were separated by a polypropylene spacer, and the cell was stored in a temperature cabinet (LU-114, ESPEC) at 50 °C for several days to stabilize the symmetric cell. Then, impedance spectra were measured prior to the potentiostatic polarization. The current was monitored while a potentiostatic polarization was applied to the cell with a potential step of 10 mV. After a steady current was observed, impedance spectra were measured again. The following equation gives the transference number,

$$t_{\mathrm{Li}^+} = [I_\mathrm{ss}(\Delta V - I_0R_0)]/[I_0(\Delta V - I_\mathrm{ss}R_\mathrm{ss})] \quad (1)$$

where ΔV is the applied potential ($\Delta V = 10$ mV), I_0 is the initial current of the potentiostatic polarization, I_SS is the steady state current of the polarization, R_0 is the interfacial resistance before the polarization, and R_SS is the steady state interfacial resistance during the polarization.

2.5 Charge/discharge test of the Li/PCEO$_5$LiTFSA/LiFePO$_4$ cell

The Li|PCEO$_5$LITFSA|LiFePO$_4$ cell was prepared using the previously reported PE based on PCEO.[17] Lithium metal foil (diameter: 10 mm, Honjo Metal Co., Ltd.) was used as the negative electrode. The positive electrode was composed of LiFePO$_4$ as the active material (theoretical capacity: 170 mA h g^{-1}), acetylene black (AB) as the conductive supporting agent, polyvinylidene fluoride (PVdF), and PCEO$_5$LiTFSA as the binder at a weight ratio of LiFePO$_4$: AB : PVdF : PCEO$_5$LiTFSA = 75 : 15 : 10 : 1. The materials were suspended in *N*-methylpyrrolidone, and the slurry was coated onto a stainless steel (SUS) foil. After drying at 60 °C for 4 h, the electrode was cut into a circular shape (10 mm in diameter) and compressed at 2 kN for 15 min. LiFePO$_4$ was loaded on the electrode (2 mg cm^{-2}). A porous glass filter paper (GA-55, ADVANTEC) was used as a mechanical electrolyte support because the PE used in this study was not self-standing (it was not crystalline and had a low T_g). PCEO$_5$LiTFSA was heated to 130 °C and infiltrated into the glass filter paper under vacuum. A 2032-type coin cell was assembled using the above electrodes and the PE in the Ar-filled glove box.

A charge/discharge test was performed with a charge–discharge unit (HJ1020mSD8, Hokuto Denko). The temperature of the cell was maintained at 70 °C in an aluminum bath during the charge/discharge test. The rate capability of the cell was investigated by changing the charge–discharge rate (0.05, 0.1, 0.2, 0.5, 1, and 2C). The charging cutoff voltage was set to 3.9 V to avoid electrolyte oxidation, while the discharging cutoff voltage was 2.5 V.

3. Results and discussion

3.1 Thermal properties

Table 1 summarizes the molecular weights (M_n and M_w), polydispersity index ($M_\mathrm{w}/M_\mathrm{n}$), and T_g of pure PCHO, as determined from the GPC and DSC measurements. The reported data for PCEO are also listed for comparison. PCEO is a semi-crystalline polymer with a small melting peak at 55 °C and T_g at −18.3 °C.[17] Although one may expect that the ethyl group on the main chains of PCEO would sterically hinder chain packing to form a crystalline phase, it rather assisted the formation of a small crystalline domain in PCEO. In contrast, the DSC thermogram of PCHO did not contain an endothermic peak corresponding to the melting of the crystalline domain, suggesting that PCHO is amorphous. The T_g of PCHO is lower than that of PCEO (−18.3 °C), but higher than the reported T_g of plain poly(trimethyl oxide), –(CH$_2$CH$_2$CH$_2$O)$_n$–, (−71 °C).[20] The presence of side chains could increase T_g, and PCEO having the nitrile and ethyl side chains showed higher T_g values because of enhanced intermolecular interactions. Considering the thermal behavior, PCHO is expected to be more favorable than PCEO for ion transport because of its non-crystallinity and lower T_g.

Fig. 2 shows the salt concentration dependence of T_g for PCEO$_a$LiTFSA and PCHO$_a$LiTFSA: T_g of the PEs values were plotted as a function of the molar ratio of possible interaction sites and LiTFSA, ([O] + [CN])/[Li]. For comparison, the reported T_g data of PEO$_a$LiTFSA,[21] which is the most widely studied PE for lithium secondary batteries, are also shown in Fig. 2. In PEO-based electrolytes, T_g increases as the salt concentration increases. This is due to ionic cross-linking formed by multidentate coordination of the main chain ether groups to Li$^+$ ions, in which the polymer segmental motion is highly restricted. In contrast, we report that the T_g value of PCEO decreases as the salt concentration increases.[16,17] This plasticizing effect is due to relaxation of dipole–dipole interactions between the nitrile groups of PCEO in the presence of the Li salt. This plasticization with the addition of Li salt is not limited to PCEO, but has also been reported for polyacrylonitrile,[22] and

Table 1 Molecular weights (M_n and M_w), polydispersity index (M_w/M_n), and thermal characteristic (T_g and melting point, T_m) of PCHO. Data for PCEO were obtained from ref. 17

	Molecular weight			Thermal characteristics	
	M_n [g mol^{-1}]	M_w [g mol^{-1}]	M_w/M_n [—]	T_g [°C]	T_m [°C]
PCEO	4.56×10^4	1.08×10^5	2.37	−18.3	55.0
PCHO	2.86×10^4	7.94×10^4	2.78	−30.9	Not observed

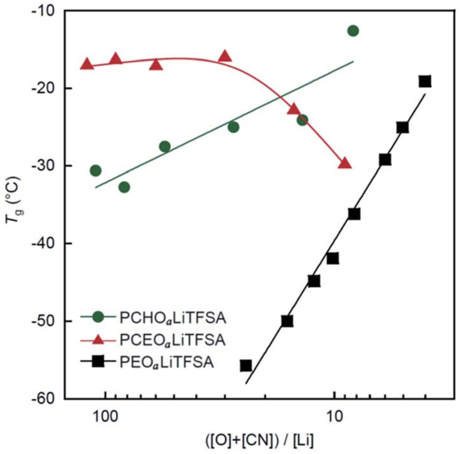

Fig. 2 T_g as a function of the molar ratio of possible interaction sites and LiTFSA in the PEs ([O] + [CN])/[Li] for PCHO$_a$LiTFSA, PCEO$_a$LiTFSA, and PEO$_a$LiTFSA. T_g values for PCEO$_a$LiTFSA and PEO$_a$LiTFSA were obtained from ref. 17 and 21, respectively.

polyethylene carbonate.[23] In the context of free volume theory for amorphous materials,[24,25] the reduction in T_g by the addition of Li salt implies that the free volume in the system increases upon Li$^+$ ion coordination. This is likely the case because sterically hindered Li$^+$ coordination with the main chains and preferential Li$^+$ coordination with polar side chains would result in a more loosely-packed segmental arrangement.

For newly synthesized PCHO, T_g increases with increasing salt concentration, although the increase in T_g is gentler than that of PEO$_a$LiTFSA. This suggests that PCHO forms an ionically cross-linked structure in the presence of LiTFSA, but the cross-linking density is not as dense as that in PEO$_a$LiTFSA. The differences in the thermal behavior between PCEO$_a$LiTFSA and PCHO$_a$LiTFSA suggest that the ethyl group on the polyoxetane main chains plays an important role in the Li$^+$ ion coordination structure and the resultant thermal behavior in the PEs. The prepared PEs (PCEO$_a$LiTFSA and PCHO$_a$LiTFSA) were not a rubbery solid, but were a highly viscous solution due to the low crystallinity and the lower T_g. However, a self-standing membrane can be readily formed by introducing robust cross-linking points into the polymers as reported in the literature.[26–28]

3.2 Ionic conductivity

In Fig. 3, the ionic conductivities of PCHO$_a$LiTFSA at 30 °C and 70 °C are plotted as a function of the molar ratio of LiTFSA to the repeating monomer unit, 1/a (relevant to the salt concentration). For comparison, the conductivity data for PCEO$_a$LiTFSA are also shown in the same figure. Furthermore, the molar conductivity is also shown in the ESI (Fig. S1†). At low values of 1/a (*i.e.*, low salt concentration), the ionic conductivity of PCHO$_a$LiTFSA is higher than that of PCEO$_a$LiTFSA. This is attributed to the high mobility of ions in PCHO$_a$LiTFSA. As shown in Fig. 2, a lower T_g value is evidently responsible for the faster segmental motion and the lower local viscosity of PCHO$_a$LiTFSA. The ionic conductivity increases for both PEs with increasing 1/a (*i.e.*, increasing salt concentration), except for PCHO$_a$LiTFSA at the highest 1/a. However, PCHO$_a$LiTFSA shows only a small change in conductivity and a continuous decrease in molar conductivity with increasing 1/a (Fig. S1†). The contribution of the increase in the charge carrier would be negated by the increase in T_g with the addition of Li salt (as shown in Fig. 2), which would account for the marginal change in the conductivity and the decrease in the molar conductivity at higher 1/a. The Li salt concentration dependence of the PCHO$_a$LiTFSA conductivity qualitatively agrees with that for the PEO-based PEs; the change in conductivity and molar conductivity fall within one order of magnitude, which is comparable to that for PEO-based PEs.[29,30] Therefore, this typical change is predominantly due to a reduction in mobility by the formation of an ionically cross-linked structure. The ever-increasing conductivity for PCEO$_a$LiTFSA suggests again that the presence of the ethyl group can inhibit the formation of the cross-

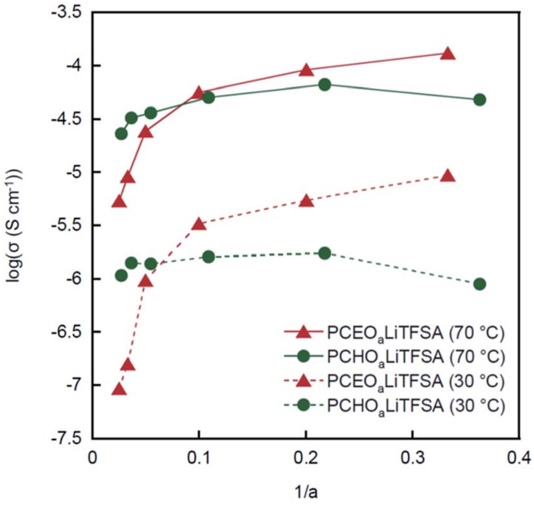

Fig. 3 Ionic conductivity of the PEs as a function of LiTFSA content (1/a) at 30 °C and 70 °C.

linked structures by Li^+ ion coordination with the ether main chains.

The temperature dependent conductivity (σ) was also measured to elucidate the ionic conduction mechanism in PCEO$_a$LiTFSA and PCHO$_a$LiTFSA, as shown in Fig. S2.† The Arrhenius plots of the conductivity show non-linear behavior with a curvature that is generally observed for amorphous PEs, and are well described by an empirical expression in relation to the Vogel–Tammann–Fulcher equation,[5]

$$\sigma = AT^{-1/2}\exp\left[\frac{-B}{R(T-T_0)}\right] \tag{2}$$

where A is a fitting parameter relevant to the number of charge carriers, B is the pseudo activation energy of ionic conduction, R is the gas constant, and T_0 is an ideal glass transition temperature. Because T_0 is typically 30–50 K below T_g for many cases, we defined $T_0 = T_g - 50$ K for fitting the conductivity data according to the previous report.[31] Table 2 shows the obtained parameters for PCEO$_a$LiTFSA and PCHO$_a$LiTFSA. PCEO$_a$LiTFSA with low Li salt concentrations (a = 20, 30, and 40) are crystalline; therefore, these compounds are not included in the fitting analysis.

The A parameter tends to increase with increasing salt concentration in each PE, indicating that the number of effective charge carriers increases with the addition of the Li salt. The A value of PCHO$_a$LiTFSA was higher than that of PCEO$_a$LiTFSA at the same a value. The absence of ethyl groups in PCHO may result in a higher polarity in the PE, which can promote ionic dissociation of the Li salt, leading to the higher A value for PCHO$_a$LiTFSA. PCHO$_a$LiTFSA shows slightly larger values of B than PCEO$_a$LiTFSA, indicating that PCHO$_a$LiTFSA has a little higher activation barrier for ion exchange between the coordination sites in the PEs. This implies that Li^+ ion coordination is more stabilized in PCHO than in PCEO, and Li^+ ions are more tightly trapped by the multi-dentate polyether groups in PCHO$_a$LiTFSA.

In our previous work, we reported that the parameters A and B for PCEO$_a$LiBF$_4$ and PCEO$_a$LiBF$_4$ show smaller A and larger B values than those of PCEO$_a$LiTFSA at the same a value.[15] It seems that the more associative character and smaller size of LiBF$_4$ are responsible for the smaller A value and larger B value. The B value of the PEO-based PEs dramatically changes with respect to the salt concentration and anion species,[32] and $B = 24$ kJ mol^{-1} was reported for PEO$_{12}$LiTFSA.[33] Hence, the smaller B values of PCEO$_a$LiTFSA and PCHO$_a$LiTFSA than that of the PEO-based PEs suggest that ion migration is promoted more in PCEO and PCHO by preferential Li^+ ion coordination with the nitrile side chains.

Table 2 The fitting parameters for PCEO$_a$LiTFSA and PCHO$_a$LiTFSA

Polymer	a	A (S cm^{-1} K$^{1/2}$)	B (kJ mol^{-1})
PCEO	10	1.21	7.96
	5	3.19	8.84
	3	5.75	9.49
PCHO	40	2.21	10.7
	30	4.97	11.5
	20	4.88	10.9
	10	9.34	11.1
	5	11.9	11.6
	3	9.86	10.2

3.3 Coordination structure of Li^+ ions

Raman spectroscopic measurements were carried out to investigate the coordination structure formed in PEs. The Raman spectra of the nitrile group (2200–2320 cm^{-1}) is shown in Fig. 4. A symmetric peak that can be assigned to the stretching vibration of nitrile groups is observed at 2249 cm^{-1} for pure PCHO. However, another peak emerges at higher wavenumber in the presence of LiTFSA. This is indicative of Li^+ ion coordination with the nitrile groups in PCHO$_a$LiTFSA. The Raman spectra in this region show an isosbestic point at 2255 cm^{-1} (except that for PCHO$_3$LiTFSA), indicating that two species (*i.e.*, free and bound nitrile groups) co-exist. Here, each spectrum was further analyzed using the same procedure as that in our previous report,[17] and each was deconvoluted into four bands at 2249, 2253, 2264, and 2277 cm^{-1}, as shown Fig. 4b. The peaks at 2249 and 2253 cm^{-1} are assigned to vibrations of uncoordinated (free) nitrile groups, whereas the peaks at 2264 and 2277 cm^{-1} are due to nitrile groups bound to Li^+ ions. The intensity of a peak at x cm^{-1} is given as $I_{x(\mathrm{CN})}$. To quantitatively determine the coordination number of the nitrile group (n_{CN}), the relationship between the slope and intercept of the linear function plotted as $I_{\mathrm{f(CN)}}/c_{\mathrm{Li}}$ *vs.* a was analyzed using the following relationship,

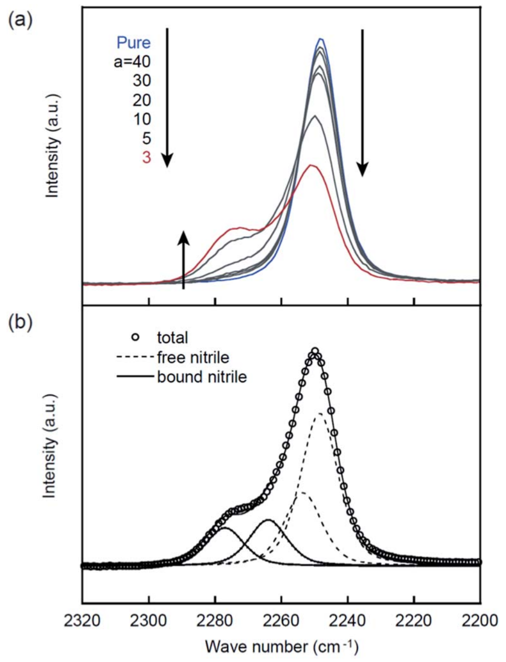

Fig. 4 Raman spectra of the nitrile group in PCHO$_a$LiTFSA in the frequency range of 2200–2320 cm^{-1} at room temperature. (a) Dependence on Li salt concentration (pure and a = 3–40) and (b) typical result upon deconvolution of the spectrum for a = 5.

$$I_{\mathrm{f(CN)}}/c_{\mathrm{Li}} = J_{\mathrm{f(CN)}}(a - n_{\mathrm{CN}}) \quad (3)$$

where $I_{\mathrm{f(CN)}}$ is the sum of the integrated intensities of the lower two bands ($I_{\mathrm{f(CN)}} = I_{2249\mathrm{(CN)}} + I_{2253\mathrm{(CN)}}$), and $J_{\mathrm{f(CN)}}$ is the molar Raman scattering coefficient of the free nitrile moieties. For highly concentrated PCHO$_3$LiTFSA ($a = 3$), the Raman spectrum deviates from the isosbestic point and shifts to a lower wavenumber, suggesting that the Li$^+$ ion coordination structure is different from that of the others. Therefore, the data for PCHO$_3$LiTFSA are excluded from the fitting analysis.

Fig. 5 shows the result of the linear least-square fitting to eqn (3) for the nitrile group in PCHO$_a$LiTFSA. From the good linear relationship in Fig. 5, we could determine the coordination number of the nitrile group in PCHO$_a$LiTFSA ($n_{\mathrm{CN}} = 0.81 \pm 0.40$), which is smaller than the reported n_{CN} of PCEO$_a$LiTFSA (0.93 ± 0.7).[17] Thus, Li$^+$ ion coordination with the nitrile groups is less pronounced in PCHO$_a$LiTFSA. The Li$^+$ ion was probably more preferentially coordinated with the ether groups by the absence of the steric hindrance of the ethyl groups on the main chains in PCHO$_a$LiTFSA.

The Raman spectra corresponding to the CF$_3$ bending vibration coupled with the S–N stretching vibration of the TFSA anion are shown in Fig. 6. To investigate the Li$^+$ ion coordination with the TFSA anions, these Raman spectra were further deconvoluted into two peaks at 739 and 745 cm^{-1} using the same method as that used in the previous work.[17] The peak at 739 cm^{-1} can be assigned to TFSA in the form of a free or solvent separated ion pair, whereas the peak at 745 cm^{-1} corresponds to TFSA directly bound to Li$^+$ ions in the form of a contact ion pair or aggregates. The respective peak intensities ($I_{739\mathrm{(TFSA)}}$ and $I_{745\mathrm{(TFSA)}}$) were used to determine the coordination number of TFSA anions (n_{TFSA}) according to the following equations,[34]

$$0.9I_{739\mathrm{(TFSA)}} + I_{745\mathrm{(TFSA)}} = J_{745\mathrm{(TFSA)}}c_{\mathrm{Li}} \quad (4)$$

$$I_{745\mathrm{(TFSA)}} = J_{745\mathrm{(TFSA)}}n_{\mathrm{TFSA}}c_{\mathrm{Li}} \quad (5)$$

As shown in Fig. 7, a relatively good linear relationship is obtained for both cases, and the coordination number for PCHO$_a$LiTFSA is estimated as $n_{\mathrm{TFSA}} = 0.16 \pm 0.01$ using the two linear fitting results. This value is nearly half the reported n_{TFSA} value for PCEO$_a$LiTFSA (0.30 ± 0.04).[17] The Raman spectra corresponding to the ether groups (800–900 cm^{-1}) are very complicated because various vibrational modes are involved in this range; therefore, the coordination number of the ether groups could not be determined from the spectroscopic analysis. Given the total coordination number of Li$^+$ ions (generally 4–5)[35,36] and the values of n_{CN} and n_{TFSA}, more ether groups on the main chains can be anticipated to coordinate to Li$^+$ ions in PCHO$_a$LiTFSA than in PCEO$_a$LiTFSA. This can form a cross-linked structure based on the main chains in PCHO$_a$LiTFSA, which is consistent with the experimental observations: T_g increases with the addition of Li salt (Fig. 2) and the slightly higher values for the B parameter for ionic conduction (Table 2). The ethyl groups in PCEO likely sterically hinder Li$^+$ ion

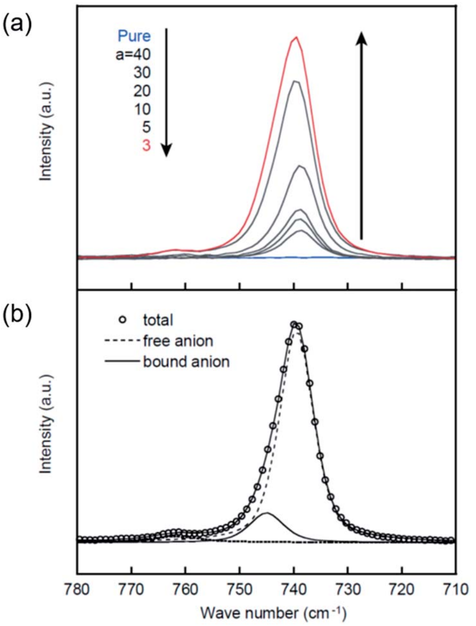

Fig. 6 Raman spectra in PCHO$_a$LiTFSA in the frequency range of 710–780 cm^{-1} at room temperature. (a) Dependence on Li salt concentration (pure and $a = 3$–40) and (b) typical result upon deconvolution of the spectrum for $a = 5$.

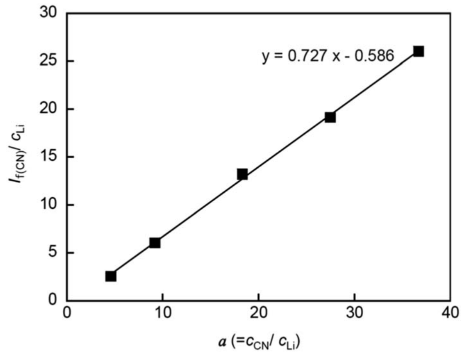

Fig. 5 $I_{\mathrm{f(CN)}}/c_{\mathrm{Li}}$ plotted as a function of a ($=c_{\mathrm{CN}}/c_{\mathrm{Li}}$) for PCHO$_a$LiTFSA. The solid line represents the least-square linear fitting.

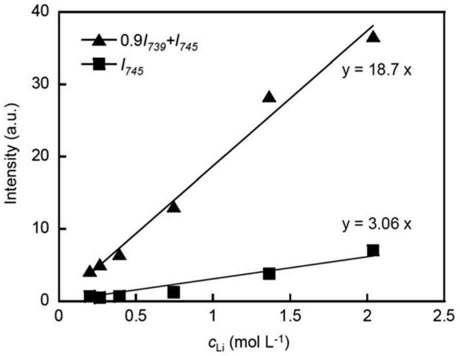

Fig. 7 $I_{\mathrm{f(CN)}}/c_{\mathrm{Li}}$ plotted as a function of a ($=c_{\mathrm{CN}}/c_{\mathrm{Li}}$) for PCHO$_a$LiTFSA. The solid line represents the least-square linear fitting.

coordination with the ether groups, which promotes Li^+ ion coordination with the nitrile side chains and TFSA anions, as evidenced by the larger n_{CN} and n_{TFSA} values for PCEO$_a$LiTFSA.

3.4 Li^+ ion transference number

To elucidate the transport properties of the Li^+ ions in each PE, the transference number (t_{Li^+}) was measured using an electrochemical method.[19] As this value increases beyond 0.5, Li^+ migration proceeds at a faster rate relative to TFSA anions in the PEs. The experimental data are shown in the ESI (Fig. S3 and S4†). t_{Li^+} values of 0.59 and 0.40 are obtained for PCEO$_5$LiTFSA and PCHO$_5$LiTFSA, respectively. The lower t_{Li^+} value for PCHO$_5$LiTFSA indicates that the migration of Li^+ ions is more restricted in PCHO$_5$LiTFSA, and corroborates the more-pronounced coordination with the ether groups, whereby the mobility of Li^+ ions is coupled with the segmental motion of the ether main chains. The t_{Li^+} values for PCEO$_5$LiTFSA and PCHO$_5$LiTFSA are much larger than those for typically studied PEs, such as PEO$_a$LiTFSA (typically < 0.2).[37,38] Li^+ ion exchange occurs more frequently between the mono-dentate nitrile side chains and the counter anions than between the multidentate polyethers on the main chains; therefore, the Li^+ ion can travel more effectively *via* side chain coordination and site exchange.

3.5 Charge/discharge tests

Based on the comparative study shown above, we found that PCEO$_5$LiTFSA exhibits higher Li^+ ion transport properties. Here, we assembled a lithium-ion half-cell, Li|PCEO$_5$LiTFSA|$LiFePO_4$, with PCEO$_5$LiTFSA as an electrolyte to study whether the polyoxetane–PEs are indeed applicable to Li secondary batteries. No capacity was observed at 30 °C even at very low charge–discharge rate (0.05C), probably due to low ionic conductivity of PCEO$_5$LiTFSA. The preliminary charge/discharge test from 2.5–4.0 V at 70 °C causes an unexpected charging plateau and an apparent overcharge is observed around 3.95 V (Fig. S5†). We previously reported that the electrochemical window of PCEO$_5$LiTFSA is ~4.0 V *vs.* Li/Li^+ on stainless steel electrodes.[17] This indicates the oxidative decomposition of PCEO$_5$LiTFSA on the cathode at this potential. Therefore, a further charge/discharge test was performed in the range of 2.5–3.9 V at 70 °C. The charge–discharge curves and cycle performance with different charge–discharge rates are shown in Fig. 8. The obtained capacities are approximately 100 mA h g^{-1}, even with a low charge–discharge current density at 0.05C, and are much lower than the theoretical capacity of $LiFePO_4$ (170 mA h g^{-1}). This is predominantly due to the insufficient electrode/electrolyte interface in the composite cathode, even though PCEO$_5$LiTFSA is combined with the composite cathode as the co-binder. To construct better electron/ion pathways, the material composition and the fabrication procedure of the cathode must be further optimized. With an increasing charge–discharge rate, the capacity drastically decreases and the overvoltage increases. In particular, almost no capacity is delivered at rates above 1C. This is probably caused by the low ionic conductivity of PCEO$_5$LiTFSA. However, the cell shows a relatively stable cycle performance with only a slight capacity loss at the same rate and high coulombic efficiency of ~99.5%, suggesting that the electrochemical reaction at the positive electrolyte ($LiFePO_4 \rightleftarrows FePO_4 + Li^+ + e^-$) is highly reversible in PCEO$_5$LiTFSA. Thus, these results suggest that the polyoxetane-based PEs with nitrile functionality are applicable to Li secondary batteries.

4. Conclusions

The steric effect of the ethyl group of polyoxetane-based PEs with nitrile side chains was clarified by comparing the thermal properties, Li^+ ion coordination, and ion transport properties of PCHO$_a$LiTFSA and PCEO$_a$LiTFSA. As the Li salt concentration increased, T_g increased for PCHO$_a$LiTFSA; this behavior is analogous to that of well-studied PEO-based PEs. Conversely, T_g decreased with increasing salt concentrations for PCEO$_a$LiTFSA. Correspondingly, the ionic conductivity of PCHO$_a$LiTFSA was lower than that of PCEO$_a$LiTFSA in the high salt concentration region, mainly because of the higher microviscosity. The Li^+ ion coordination structure was investigated using Raman spectroscopy, which revealed that the mixed coordination with ether groups, nitrile side chains, and TFSA anions occurred in both PCHO$_a$LiTFSA and PCEO$_a$LiTFSA;

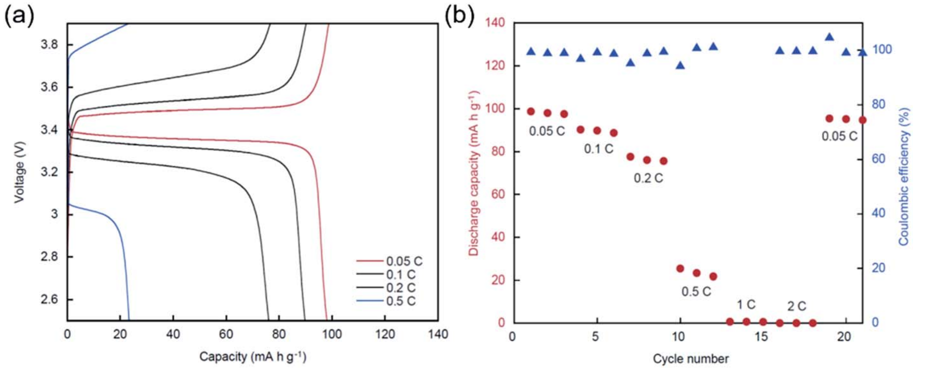

Fig. 8 (a) Charge/discharge curves and (b) cycle properties of the Li/PCEO$_5$LiTFSA/$LiFePO_4$ cell at 70 °C. The measurements were carried out in the range of 2.5–3.9 V (1C = 356 μA cm^{-2}). Coulombic efficiencies exceeded 110% at 1C and are not shown in the figure because of the negligible discharge capacities that were higher than the charge capacities recorded in the charge–discharge unit.

however, the ether groups were more prone to coordinating with Li$^+$ ions in PCHO$_a$LiTFSA. The more preferential Li$^+$ ion coordination with the ether groups resulted in a more pronounced cross-linking of the main chains with Li$^+$ ions, leading to an increase in T_g and less effective Li$^+$ ion transport (*i.e.*, lower conductivity and t_{Li^+}) in PCHO$_a$LiTFSA. In other words, the ethyl group played a pivotal role in enhancing the Li$^+$ ion transport by sterically inhibiting Li$^+$ ion coordination with the ether main chains of the polyoxetanes. In addition, the Li–LiFePO$_4$ cell using PCEO$_5$LiTFSA showed a reversible charge–discharge with a relatively stable cycle ability and high coulombic efficiency. Although the conductivity values of PCHO$_a$LiTFSA and PCEO$_a$LiTFSA (on the order of 10^{-6} to 10^{-5} S cm^{-1} at 30 °C) were not sufficient for practical applications in solid-state Li secondary batteries, this work could provide insight into the molecular design of PEs for pursuing a high ionic conductivity at a level comparable to that of liquid electrolytes, in association with a high Li$^+$ ion transference number that rivals that of inorganic solid electrolytes.

Conflict of interest

There are no conflicts to declare.

Acknowledgements

This study was supported by JSPS KAKENHI (No. 16H06053 for KU and No. 16H04647 for HT).

References

1 K. S. Ngai, S. Ramesh, K. Ramesh and J. C. Juan, *Ionics*, 2016, **22**, 1259–1279.

2 C. Sun, J. Liu, Y. Gong, D. P. Wilkinson and J. Zhang, *Nano Energy*, 2017, **33**, 363–386.

3 Y. Kato, S. Hori, T. Saito, K. Suzuki, M. Hirayama, A. Mitsui, M. Yonemura, H. Iba and R. Kanno, *Nat. Energy*, 2016, **1**, 16030.

4 Y. Zhang, J. Lai, Y. Gong, Y. Hu, J. Liu, C. Sun and Z. L. Wang, *ACS Appl. Mater. Interfaces*, 2016, **8**, 34309–34316.

5 E. Quartarone and P. Mustarelli, *Chem. Soc. Rev.*, 2011, **40**, 2525–2540.

6 L. Long, S. Wang, M. Xiao and Y. Meng, *J. Mater. Chem. A*, 2016, **4**, 10038–10069.

7 M. Tatsumisago, M. Nagao and A. Hayashi, *J. Asian Ceram. Soc.*, 2013, **1**, 17–25.

8 P. V. Wright, *Br. Polym. J.*, 1975, **7**, 319–327.

9 D. E. Fenton, J. M. Parker and P. V. Wright, *Polymer*, 1973, **14**, 589.

10 D. W. Dees, V. S. Battaglia and A. Bélanger, *J. Power Sources*, 2002, **110**, 310–320.

11 J. B. Kerr, S. E. Sloop, G. Liu, Y. B. Han, J. Hou and S. Wang, *J. Power Sources*, 2002, **110**, 389–400.

12 M. A. Webb, B. M. Savoie, Z.-G. Wang and T. F. Miller III, *Macromolecules*, 2015, **48**, 7346–7358.

13 H. Tsutsumi and A. Suzuki, *Solid State Ionics*, 2014, **262**, 761–764.

14 R. Shibutani and H. Tsutsumi, *J. Power Sources*, 2012, **202**, 369–373.

15 Y. Nakano and H. Tsutsumi, *Solid State Ionics*, 2014, **262**, 774–777.

16 Y. Shintani and H. Tsutsumi, *J. Power Sources*, 2010, **195**, 2863–2869.

17 R. Sai, K. Ueno, K. Fujii, Y. Nakano, N. Shigaki and H. Tsutsumi, *Phys. Chem. Chem. Phys.*, 2017, **19**, 5185–5194.

18 K. Kubota, K. Tamaki, T. Nohira, T. Goto and R. Hagiwara, *Electrochim. Acta*, 2010, **55**, 1113–1119.

19 J. Evans, C. A. Vincent and P. G. Bruce, *Polymer*, 1987, **28**, 2324–2328.

20 E. Pérez, M. A. Gómez, A. Bello and J. G. Fatou, *Colloid Polym. Sci.*, 1983, **261**, 571–576.

21 M. Perrier, S. Besner, C. Paquette, A. Vallée, S. Lascaud and J. Prud'homme, *Electrochim. Acta*, 1995, **40**, 2123–2129.

22 M. Forsyth, J. Sun and D. R. Macfarlane, *Solid State Ionics*, 1998, **112**, 161–163.

23 K. Kimura, J. Motomatsu and Y. Tominaga, *J. Phys. Chem. C*, 2016, **120**, 12385–12391.

24 R. G. Larson, *The Structure and Rheology of Complex Fluids*, OUP, USA, 1999.

25 R. P. White and J. E. G. Lipson, *Macromolecules*, 2016, **49**, 3987–4007.

26 R. Bouchet, S. Maria, R. Meziane, A. Aboulaich, L. Lienafa, J.-P. Bonnet, T. N. T. Phan, D. Bertin, D. Gigmes, D. Devaux, R. Denoyel and M. Armand, *Nat. Mater.*, 2013, **12**, 452–457.

27 L. Porcarelli, C. Gerbaldi, F. Bella and J. R. Nair, *Sci. Rep.*, 2016, **6**, 19892.

28 S. Choudhury, R. Mangal, A. Agrawal and L. A. Archer, *Nat. Commun.*, 2015, **6**, 10101.

29 A. Vallée, S. Besner and J. Prud'Homme, *Electrochim. Acta*, 1992, **37**, 1579–1583.

30 L. Edman, M. M. Doeff, A. Ferry, J. Kerr and L. C. De Jonghe, *J. Phys. Chem. B*, 2000, **104**, 3476–3480.

31 K. B. M. Isa, Z. Osman, A. K. Arof, L. Othman, N. H. Zainol, S. M. Samin, W. G. Chong and N. Kamarulzaman, *Solid State Ionics*, 2014, **268**, 288–293.

32 C. D. Robitaille and D. Fauteux, *J. Electrochem. Soc.*, 1986, **133**, 315–325.

33 S. Das and A. Ghosh, *J. Appl. Phys.*, 2015, **117**, 174103.

34 Y. Umebayashi, T. Mitsugi, S. Fukuda, T. Fujimori, K. Fujii, R. Kanzaki, M. Takeuchi and S.-I. Ishiguro, *J. Phys. Chem. B*, 2007, **111**, 13028–13032.

35 W. A. Henderson, N. R. Brooks and V. G. Young, *J. Am. Chem. Soc.*, 2003, **125**, 12098–12099.

36 Y. Kameda, Y. Umebayashi, M. Takeuchi, M. A. Wahab, S. Fukuda, S.-i. Ishiguro, M. Sasaki, Y. Amo and T. Usuki, *J. Phys. Chem. B*, 2007, **111**, 6104–6109.

37 K. Timachova, H. Watanabe and N. P. Balsara, *Macromolecules*, 2015, **48**, 7882–7888.

38 M. Chintapalli, K. Timachova, K. R. Olson, S. J. Mecham, D. Devaux, J. M. DeSimone and N. P. Balsara, *Macromolecules*, 2016, **49**, 3508–3515.